Journal of Physics: Conference Series

PAPER • OPEN ACCESS

Measurements of gas-liquid two-phase flow dynamics using high-speed neutron imaging

To cite this article: D Ito *et al* 2023 *J. Phys.: Conf. Ser.* **2605** 012024

Journal of Physics: Conference Series **2605** (2023) 012024 doi:10.1088/1742-6596/2605/1/012024

Measurements of gas-liquid two-phase flow dynamics using high-speed neutron imaging

D Ito[1], N Odaira[1], K Ito[1], Y Saito[1], K Kurita[2] and H Iikura[2]

[1] Institute for Integrated Radiation and Nuclear Science, Kyoto University, Osaka, JAPAN
[2] Japan Atomic Energy Agency, Ibaraki, JAPAN

E-mail: ito.daisuke.5a@kyoto-u.ac.jp

Abstract. Gas-liquid two-phase flow appears in many heat-exchanging devices. The two-phase flow dynamics should be clarified to understand the phenomena in such devices. Although many measurement techniques have been applied to two-phase flow experiments, measuring the gas-liquid interfacial structure is difficult, which changes temporally and spatially. In this study, high-speed neutron imaging is used to measure two-phase flow dynamics, and the accuracy of the void fraction measurement is investigated. In high-speed neutron imaging, image blurring and distortion occur due to light and object motion intensifying. As a result, the quantitative accuracy might decrease. So, the rotating stainless-steel calibration disk, which simulates the bubble behavior in water, is observed by high-speed neutron imaging. Several noise reduction filters are tested to remove the blur and noise in the acquired images. Finally, the air-water two-phase flow is visualized by high-speed neutron imaging, and noise filtering is applied.

1. Introduction

Gas-liquid two-phase flow is a highly complex phenomenon involving the interaction between gas and liquid phases. The two-phase flow appears in many energy devices, nuclear reactors, and chemical engineering plants, and many studies have been performed to clarify the flow phenomena. Several accurate simulation techniques of two-phase flow have recently been developed; however, the validation of the simulated results needs to be improved due to less experimental data. It is challenging to measure interfacial behavior with significant spatio-temporal fluctuation, and the void fraction should be measured accurately to clarify such behavior. Void fraction measurement methods with high spatial and temporal resolutions are required to investigate such phenomena in detail. Neutron imaging is powerful for two-phase flow visualization and void fraction measurement. It can be applied to flow measurement in an opaque channel and has applicability to the heated condition [1-3]. In addition, the flow's transient behavior is observed using a high-speed camera and an image intensifier [4].

In this study, high-speed neutron imaging is applied to measure the two-phase flow dynamics, and the accuracy of the measurement is investigated. In high-speed neutron imaging, image blurring and distortion occur due to light and object motion intensifying. As a result, the quantitative accuracy might decrease. So, the rotating stainless-steel calibration disk, which simulates the bubble behavior in water, is observed by high-speed neutron imaging. Several noise reduction filters are tested to remove the blur and noise in the acquired images. Then, the air-water two-phase flow in a narrow rectangular channel is visualized by high-speed neutron imaging, and noise filtering is applied.

2. Neutron imaging facility and system

The neutron imaging experiments are performed at the thermal neutron radiography facility (TNRF) in JRR-3, Japan Atomic Energy Agency, Japan. The neutron flux at the location of the test section is 1×10^8 n/cm^2 s. The beam size is 255 mm in width and 305 mm in height. The collimator ratio (L/D) is 176. The neutron imaging system used in this study is represented in Figure 1. Neutrons transmitted in the test section are converted to optical light by a neutron scintillator ($^6LiF/ZnS$, 100 μm thickness, RC TRITEC LTD.). Then, the light is intensified by an optical image intensifier (C9547-01MOD, Hamamatsu Photonics), and the image sequence is acquired by a high-speed camera (FASTCAM Mini AX50, Photron). In the present system configuration, the field of view is 164 mm square. The pixel resolution is 160 μm/pixel. The frame rate of the high-speed camera sets at 1,000 fps in the present experiments. Consequently, approximately 26 neutrons per pixel and frame can be detected at direct beam conditions. The number might be decreased considering the test section's existence, and the detected neutrons are expected to be much less. Therefore, the image intensifier is applied in this study. However, the noise effect cannot be ignored in the present system configuration, and image restoration is required post-processing.

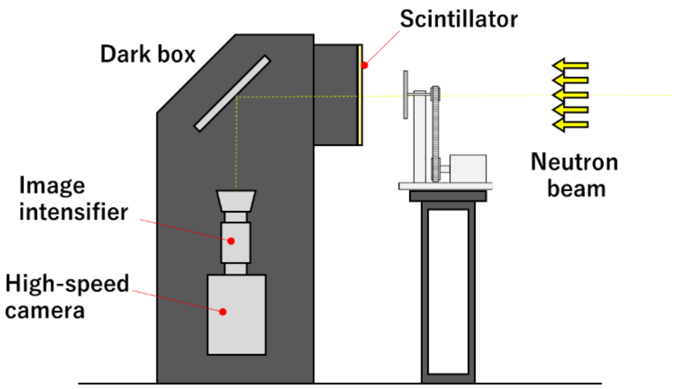

Figure 1. Schematic diagram of the neutron imaging system in TNRF.

3. Calibration disk rotation experiments

3.1. Rotation disk setup

A rotating calibration disk system is used to establish the restoration method for dynamic image sequences of high-speed neutron imaging. The schematics of the system and disk are shown in Figure 2. Five stainless-steel disks with several holes are combined, and the effect of the hole size and thickness can be investigated. The outer holes have the same diameter and different thicknesses. T denotes neutron transmission calculated from the thickness of the disk. The inner holes have different sizes. A motor controller controls the rotating frequency to change the moving velocity of the holes. The frequency is varied from 1 to 16 Hz, and the hole's velocity estimated from the position and frequency is shown in the table in Figure 2.

3.2. Neutron transmission images and spatio-temporal distributions

The neutron transmission images are estimated from the acquired image of the rotating disk and the direct beam image, and the instantaneous distributions for different rotating frequencies are represented in Figure 3. It is obvious that these images include noise. At the slow rotating velocity, it is possible to identify the small diameter holes. However, the outline of the holes becomes unclear due to the motion blur in this imaging system as the velocity increases.

Next, the spatio-temporal distributions of the neutron transmission along the center line of the upper part of the rotating disk are estimated, as shown in Figure 4. This result shows the distribution in one revolution. So, the horizontal scale is different for each rotating speed. In Figure 4(a), the small hole with a diameter of 1 mm is seen clearly. Although it is also possible to recognize the small hole in Figure 4 (b), identifying the hole size is difficult in Figure 4(c).

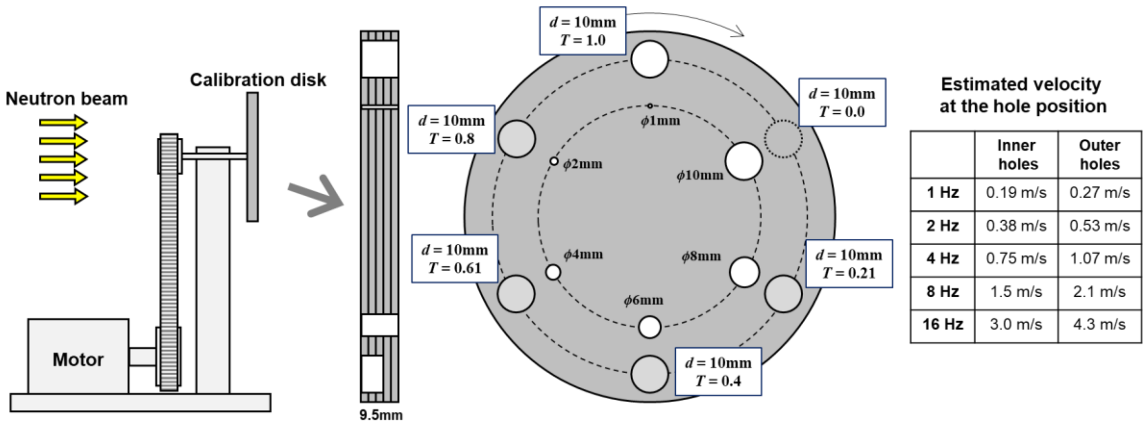

Figure 2. Schematic diagrams of the rotation disc system (left), stainless steel calibration disk with different types of holes (middle), and estimated velocity of the holes (right).

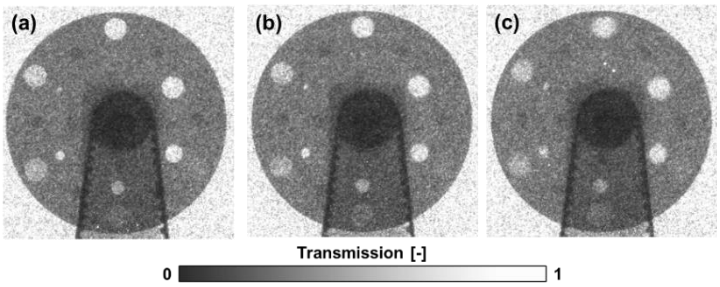

Figure 3. Neutron transmission images of the rotating disk, (a) 1 Hz, (b) 4 Hz, and (c) 16 Hz.

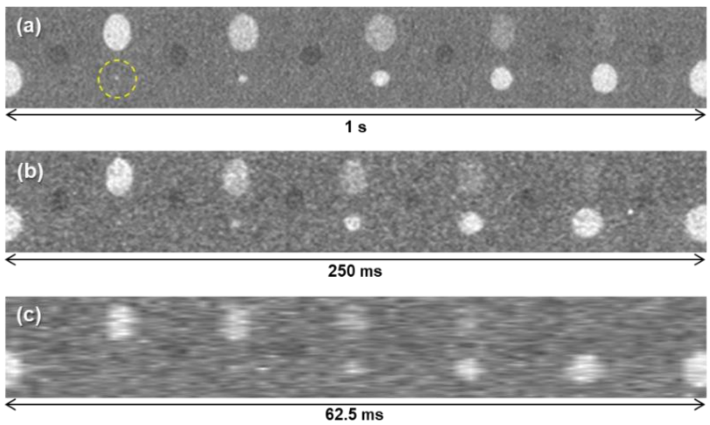

Figure 4. Spatio-temporal distributions at the rotating frequency of (a) 1 Hz, (b) 4 Hz, and (c) 16 Hz.

3.3. Denoising

In high-speed neutron imaging, image noise appears more significant than static observation. Therefore, several noise filters have been applied for dynamic image sequences. Previously, the development of the 2-D image filtering technique was remarkable. The 1-D and 3-D filtering methods are also applicable to such data. 3-D filtering can give excellent results; however, enormous calculation time is required, and applying the imaging results takes much work. We focused on the 1-D noise filter. There are also many filtering methods for 1-D signals. In this study, 1-D total variation denoising (TVD) [5,6] was applied to image sequences measured using the imaging system with the high-speed camera and the image intensifier.

$$\text{minimize}\left(\frac{1}{2}\|y-x\|_2^2+\lambda\|Dx\|_1\right) \tag{1}$$

where y is the input signal, x is the output signal, and D is the matrix of the first difference. λ is the regularization parameter which determines the degree of the filtering. The processing was performed using MATLAB, and the calculation takes 8 to 10 hours for an image sequence (1024 pixel ×1024 pixel ×3000 frame data).

The data in Figure 4(a) is processed by the TVD filter, and the filtered results are shown in Figure 5. The strength of the filtering changes by the regularization parameter. The difference between Figures 5(a) and (b) is very few. However, Figures 5(c) and (d) show sharp holes. Also, the tiny holes 1 mm in diameter can be observed in Figure 5(c) despite the unclear small hole in Figure 5(d). Thus, the next chapter applies the image denoising with the parameter λ = 500 to the observed results of the two-phase flow measurement.

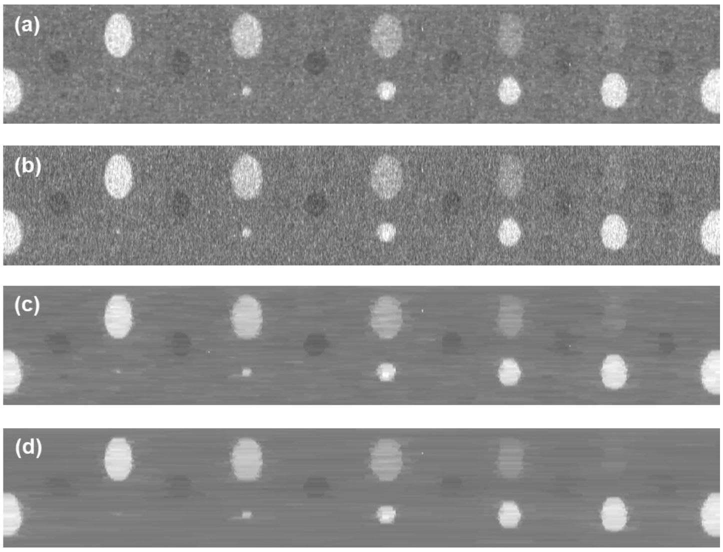

Figure 5. Evaluation of the noise reduction by TVD method, (a) not filtered, (b) λ = 100, (c) λ = 500, (d) λ = 1000.

4. Two-phase flow experiments

The experimental setup is illustrated in Figure 6. The setup consists of a test section, a pump, a water tank, and flow meters. The test section is a narrow rectangular channel with a gap of 2.8 mm and a width of 66.5 mm. Air and water flow from the bottom of the test section. The total length of the flow channel is 500 mm. The flow meter monitors the water flow rate, and the mass flow controllers control airflow. This study conducts high superficial gas velocity experiments to observe the complicated interfacial structure. The superficial gas velocity ranged from 0.9 to 4.5 m/s, and liquid velocity was constant at 0.1 m/s.

The neutron transmission images of gas single-phase, liquid single-phase, and two-phase mixture are shown in Figure 7(a) ~ (c), respectively. The image of the channel filled with water is darker than that of the empty channel because of the neutron attenuation of water. The two-phase flow image represents the instantaneous gas-phase structure in the narrow channel. The void fraction α, which is the ratio of the gas phase in the two-phase flow, is estimated from the image grayscale of the acquired images of gas and liquid single phases and two-phase mixture using the Σ-scaling method [7], as expressed in the following equations.

$$\alpha = \ln\left(\frac{G_L - G_0}{G_{LM} - G_0}\right)\Big/\ln\left(\frac{G_L - G_0}{G_G - G_0}\right) \tag{2}$$

and

$$G_0 = \frac{G_L - G_G \exp\left(-\Sigma_L \delta_L\right)}{1 - \exp\left(-\Sigma_L \delta_L\right)} \tag{3}$$

where G, Σ, and δ represent the pixel gray level, the total macroscopic cross-section, and the thickness, respectively. The subscripts L, G, and LM denote the single-liquid phase, single-gas phase, and liquid phase in the two-phase mixture. As a result, two-dimensional void fraction distribution, as shown in Figure 7(d), is obtained. Here, the neutron transmission images acquired in this system involve pincushion distortion due to the image intensifier, as shown in Figure 7(a) ~ (c). Thus, in this study, the acquired images were corrected using a calibration pattern and image processing, as shown in Figure 7(d).

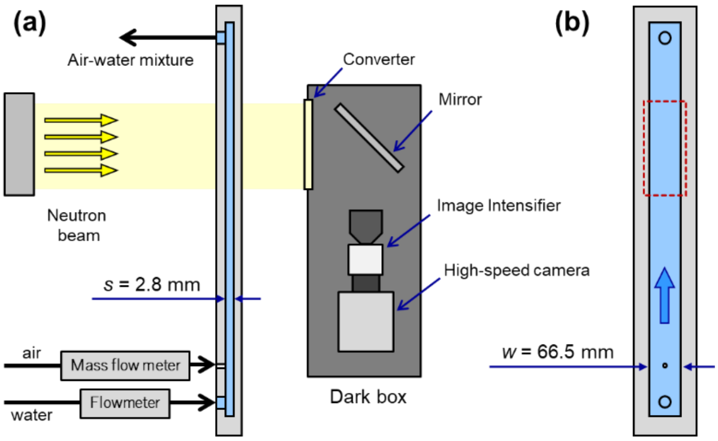

Figure 6. Experimental setup and neutron imaging system for air-water two-phase flow measurement in narrow channel; side view (a) and front view (b) of the test section.

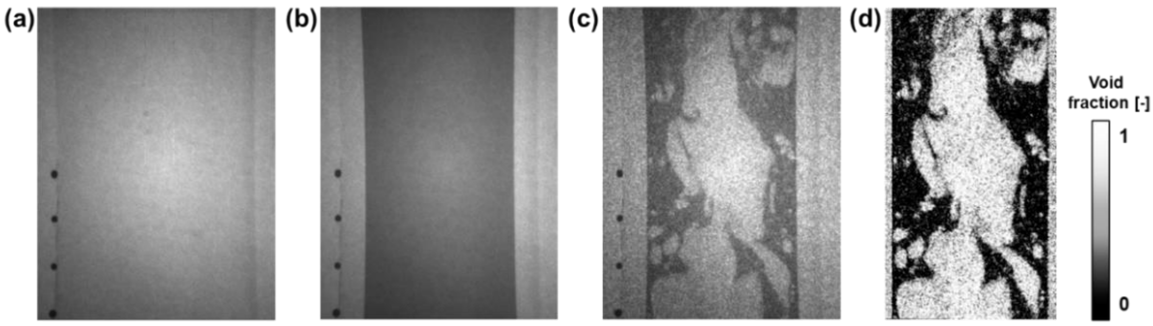

Figure 7. Neutron transmission images of gas single-phase condition (a), liquid single-phase condition (b), two-phase mixture condition (c), and estimated void fraction distribution (d).

The void fraction distributions calculated by Eq. (2) and (3) are shown in Figure 8(a). Liquid film behavior in the channel gap direction, in addition to the 2-D gas phase structure in the narrow channel, can be visualized by neutron imaging. However, the noise is significant, especially in the gas phase in the distribution. Then, the TVD filter is applied to these distributions, and the results are shown in Figure 8(b). λ = 500 in this process. The noise in the gas phase can be reduced successfully, and the edges between gas and liquid are apparent. However, this filtering amplifies the blur in the upper part of 20 ms and 30 ms in Figure 8(b).

The time-series profiles of the estimated void fraction at the center point in the distributions shown in Figure 8 are represented in Figure 9. The present denoising method can remove significant noise. Although the large fluctuation is kept in the filtered signal, the height of the signal peaks decreases slightly by the 1-D TVD. So, optimizing the filtering parameter is still required in the two-phase flow conditions, and the relation between the blur and noise should be clarified to investigate the actual two-phase flow dynamics.

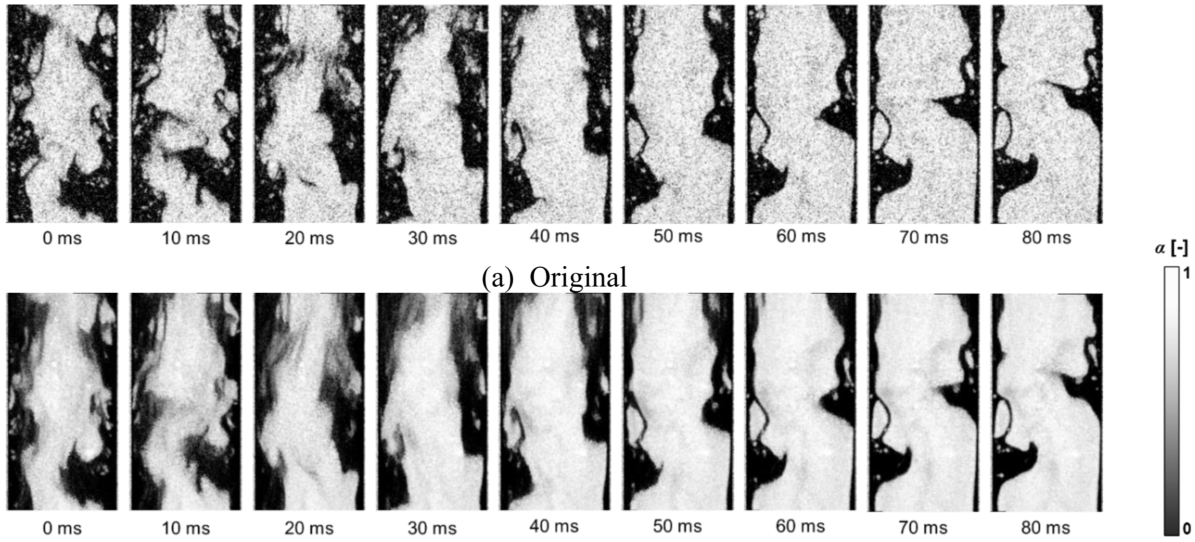

(a) Original

(b) Filtered

Figure 8. Void fraction distributions at J_G = 4.5 m/s and J_L = 0.1 m/s.

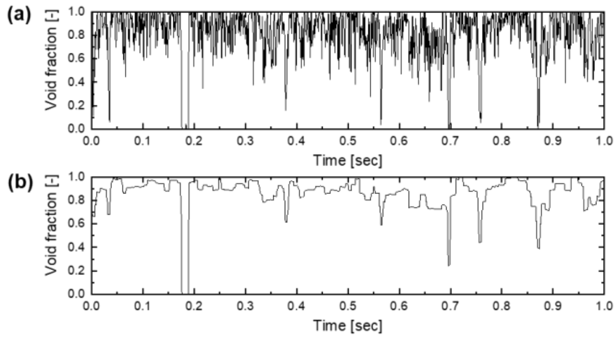

Figure 9. Void fraction signals at the center point in the distributions in Figure 8, (a) not filtered, (b) filtered.

5. Conclusions

This study investigated image degradation in high-speed neutron imaging for the detailed measurement of the two-phase flow dynamics. The noise in the present imaging was evaluated using the rotation disk system, and the possibility of noise reduction by 1-D TVD was represented. Finally, the same filtering method was applied to the results of two-phase flow measurement in the narrow rectangular channel, and the applicability of the current filter was examined. However, the filtering parameter should be optimized to enhance the dynamics observation technique using neutron imaging, and the relation between the blur restoration and denoising characteristics is clarified.

References

[1] Takenaka N, Asano H, Fujii T, Murata Y, Mochiki K, Taguchi A, Matsubayashi M and Tsuruno A 1996 *Nucl. Instrum. Methods. Phys. Res. B* **377** 153

[2] Saito Y, Mishima K, Tobita Y, Suzuki T and Matsubayashi M 2005 *Exp. Therm. Fluid Sci.* **29** 323

[3] Ami T, Umakawa H, Ito D and Saito Y 2005 *Exp. Therm. Fluid Sci.* **141** 110799

[4] Ito D and Saito Y 2020 *Mater. Research Proc.* **15** 262

[5] Kim S J 2009 *SIAM Review* **51** 339

[6] Little M A and Jones N S 2010 *2010 IEEE Int. Conf. on Acoustics, Speech and Signal Processing* 4162

[7] Mishima K and Hibiki T 1996 *Nucl. Sci. Eng.* **124** 327